Original article

Stress dependent gas-water relative permeability in gas hydrates: A theoretical model

Gang Lei[1], Qinzhuo Liao[1], Qiliang Lin[2], Liangliang Zhang[3], Liang Xue[4]⊛*, Weiqing Chen[1]

[1]*College of Petroleum Engineering & Geosciences, King Fahd University of Petroleum & Minerals, Dhahran 31261, Saudi Arabia*

[2]*Department of Civil Engineering and Engineering Mechanics, Columbia University, New York 10027, USA*

[3]*Department of Applied Mechanics, China Agricultural University, Beijing 100083, P. R. China*

[4]*State Key Laboratory of Petroleum Resources and Prospecting, China University of Petroleum (Beijing), Beijing 102249, P. R. China*

Abstract:
Research activities are currently being conducted to study multiphase flow in hydrate-bearing sediments (HBS). In this study, in view of the assumption that hydrates are evenly distributed in HBS with two major hydrate-growth patterns, i.e., pore filling hydrates (PF hydrates), wall coating hydrates (WC hydrates) and a combination of the two, a theoretical relative permeability model is proposed for gas-water flow through HBS. Besides, in this proposed model, the change in pore structure (e.g., pore radius) of HBS due to effective stress is taken into account. Then, model validation is performed by comparing the predicted results from the derived model with that from the existing model and test data. By setting the value of hydrate saturation to zero, our derived model can be reducible to the existing model, which demonstrates that the existing model is a special case of our model. The results reveal that, under the same saturation, relative permeability to water K_{rw} (or gas K_{rg}) in PF hydrates is smaller than that in WC hydrates. Moreover, the morphological characteristics of relative permeability curve (relative permeability versus gas saturation) for WC hydrate and PF hydrate are different.
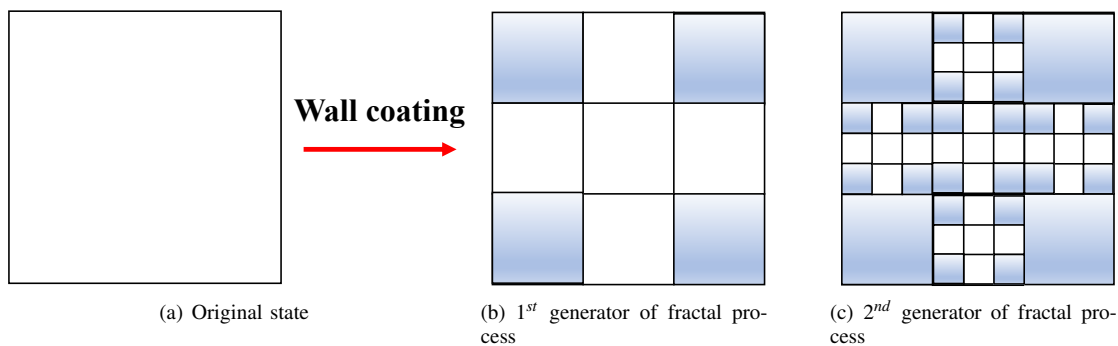
1. Introduction

Over the past few decades, gas production from hydrate-bearing sediments (HBS) has already become the focus studied and front field, and demonstrated the good development prospect. However, until now, gas hydrates have not been successfully produced (Stoll and Bryan, 1979; Aya et al., 1997; Kvenvolden, 1998a, 1998b; Sloan, 1998; Dickens, 2003; Tajima et al., 2004; Lee et al., 2010; Cui et al., 2018; Sun et al., 2018).

As suggested by previous scholars (Yousif et al., 1991; Minagawa et al., 2009; Ordonez et al., 2009; Waite et al., 2009; Kumar et al., 2010; Johnson et al., 2011; Liang et al., 2011; Dai et al., 2012; Li et al., 2014; Joseph et al., 2016), many physical properties of porous media will be strongly influenced by hydrates, which can be categorized as pore filling hydrates (PF hydrates), wall coating hydrates (WC hydrates), grain cementing hydrates (GC hydrates), and other types of

hydrates (e.g., discrete nodules, lenses, or veins) (seen in Fig. 1). Helgerud (2001) concluded that, PF hydrates nucleation occurred in the pore bodies (Fig. (1a)), WC hydrates formed on the particle surface (Fig. (1b)), GC hydrates grew at the contacts of grains (Fig. 1(c)) and other types of hydrates formed and grew randomly. Generally speaking, the actual growth type of hydrates is complex. Waite et al. (2009) and Zheng et al. (2018) suggested that hydrate-growth patterns were affected by various factors (e.g., hydrate saturation, rock petrophysical parameters, stress history, etc.). Specifically, Berge et al. (1999) and Delli and Grozic (2013, 2014) stated that, gas hydrates might change from WC hydrate to PF hydrate as hydrate saturation increased. To capture the main features of hydrates morphology in hydrate-bearing sediments (HBS) and simplify the model, many scholars (Waite et al., 2009; Singh, 2017; Singh et al., 2019a, 2019b) supposed that only PF hydrates, WC hydrates, and a combination of the two existed in the HBS. Previous studies reveal that the interspaces

(a) Pore filling hydrates   (b) Wall coating hydrates   (c) Grain cementing hydrates
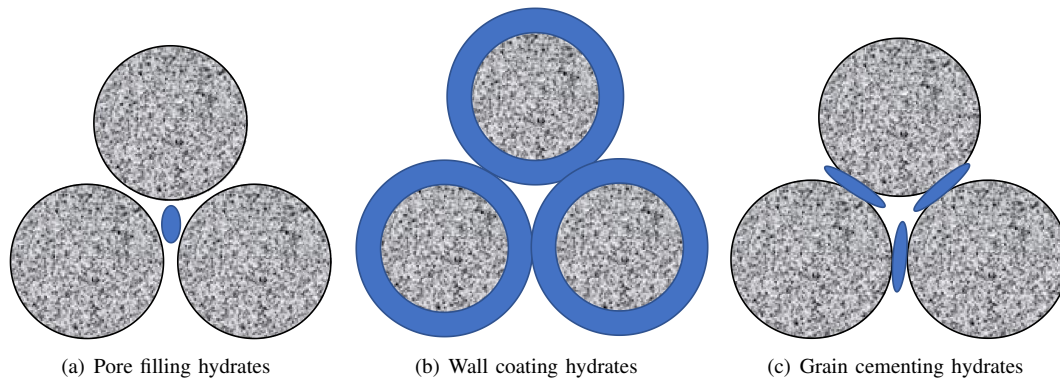
Fig. 1. Different hydrate-growth patterns in porous media: (a) PF hydrates; (b) WC hydrates; (c) GC hydrates. The grey part is rock particles, and the blue part is gas hydrates.

(a) Original state   (b) 1st generator of fractal process   (c) 2nd generator of fractal process

Fig. 2. Fractal structure of HBS with WC hydrates: (a) the 1st generator of fractal process for WC; (b) the 2nd generator of fractal process for WC. The white part is void, and the blue part is solid.

in gas hydrate sediments possess fractal characteristics (Ji et al., 1997; Fini et al., 2001; Zhao et al., 2002; Zhang et al., 2006; Kirchmeyer et al., 2015). Taking fractal WC hydrates process as an example, assuming that HBS is composed of pores and solids, a fractal HBS can be generated (Fig. 2) with the wall-coating process being repeated at increasingly small scales. As depicted in Fig. 2(a), the original state of void is simplified as a plane (Ji et al., 1997). For every fractal process of WC (Figs. 2(b) and 2(c)), the void will be divided into 9 smaller parts and 4 corner small parts will be occupied by gas hydrates.

The production potential of gas hydrates mainly depends on permeability characteristics of the bearing sediments as high permeability could promote the production rate. Furthermore, due to the gas hydrates dissociation, multi-phase flow in HBS will occur, makes it important to determine relative permeability in HBS (Zheng et al., 2018). In addition, the permeability is affected by the geomechanical conditions, e.g., effective pressure, which varies during depressurization that is one of the commonly proposed techniques in dissociating gas hydrate (Daigle, 2016). Therefore, an accurate characterization of relative permeability behavior in gas hydrate reservoirs under stress conditions has significance for sustainable gas production in deformable HBS (Nimblett and Ruppel, 2003; Waite et al., 2009; Terzariol et al., 2017; Yang et al., 2018).

Experimental determination of permeability requires the retrieval of hydrate bearing samples undisturbed, which is a challenging task. Moreover, it necessitates a precise control of pressure and temperature to ensure the maintenance of constant thermodynamic and geomechanical conditions, which is usually costly expensive. In addition, the obtained permeability is only applicable to specific hydrate-bearing medium, which becomes a cumbersome limitation (Yousif et al., 1991; Minagawa et al., 2009; Ordonez et al., 2009; Kumar et al., 2010; Johnson et al., 2011; Liang et al., 2011; Li et al., 2014; Joseph et al., 2016).

As an attractive alternative, theoretical methods for modeling and simulating relative permeability in HBS have also been developed (Wang et al., 2015; Kang et al., 2016; Mahabadi et al., 2016a, 2016b). The curve-fitting method is straightforward but contains empirical constants, whose physical meanings are not clear (Masuda et al., 1997). Kleinberg et al. (2003) derived a parallel capillary model and Kozeny grain model to study relative permeability of HBS containing two types of hydrates, i.e., PF and WC hydrates. Physically, PF hydrates nucleation occurs in the pore bodies, and WC hydrates form on the particle surface and grow gradually deep into the interior region of pores. Daigle (2016) proposed a permeability model for fractal HBS based on percolation theory. Singh et al. (2019a, 2019b) derived analytical models to investigate relative permeability in hydrate-gas-water systems with an evenly distributed pore radius. Recently, Liu et al. (2019, 2020) used fractal theory to describe pore structure of HBS, and derived fractal-based models to study permeability and relative

permeability in HBS. Moreover, Zhang et al. (2020) derived a fractal-based water permeability reduction model to explain the saturated water permeability reduction in HBS during hydrate formation. However, these models did not consider effective stress, which has been shown to influence the properties of HBS significantly (Lele et al., 2012, 2013; Liu et al., 2016). Therefore, it is significant to derive analytic methods for stress-dependent relative permeability of deformable HBS. Physically, HBS can be regarded as unsaturated porous media as shown in Fig. 1, and the strategy of research follows the transport in unsaturated porous media. In this paper, fluid flow in HBS is regarded as fluid flow in unsaturated porous media, and we derive a theoretical model for predicting stress-dependent relative permeability in HBS with the assumption that the pore structures of gas hydrate sediments under stress conditions are statistically self-similar fractals. Compared with the previous models (Daigle, 2016; Liu et al., 2019, 2020; Singh et al., 2019a, 2019b; Zhang et al., 2020), our proposed model takes effective stress into account.

In this paper, firstly, a stress dependent relative permeability model of HBS will be established. Subsequently, the derived model will be validated using the test results. Finally, the influences of relevant parameters on relative permeability will be evaluated.

2. Methodology

In this section, the analytical gas-water relative permeability model for HBS is presented. The interspaces in HBS are described using fractal geometry theory. Due to effective stress, pore radius of HBS will be narrowed, which can be quantitatively characterized with Hertz theory. More details about stress dependent pore radius and stress dependent permeability of porous media can be found in the former literature (Lei et al., 2019a, 2019b). For gas-water flow in the HBS, relative permeability will be affected by hydrate-growth patterns. Specifically, we developed a relative permeability model with the assumption that hydrates are uniformly distributed in cylindrical pores of fractal porous media with two major hydrate-growth patterns, i.e., PF hydrates, WC hydrates, and a combination of the two. In addition, for a given capillary, capillary radius does not change along the flow direction. The analytical model is derived under the following assumptions:

1. A pore with equivalent radius smaller than the critical value r_{c0} is occupied by wetting phase fluid (e.g., water phase), while this part of water cannot move and is regarded as residual water. It's supposed that in this paper residual water will not change into hydrate.

2. With regard to a capillary with a pore radius larger than r_{c0}, three phases (i.e., hydrate, gas and water) are evenly distributed in the HBS with different hydrate-growth patterns (WC hydrates, PF hydrates, and a combination of these two patterns) (Fig. 3). The rock wettability of HBS is water wet, and gas is considered as the non-wetting phase. There are no interactions between different phases.

3. With the pressure drop Δp, the steady-state, isothermal flow in pores with equivalent radius larger than r_{c0} is the continuum scale flow. Especially, gas-water two-phase flow

in pores with pore radii larger than r_{c0} can be simulated by solving continuous Navier-Stokes equations with the effects of gravity and buoyancy being neglected.

In view of the assumptions above, the residual water saturation S_{wc} in the capillary with a pore radius smaller than r_{c0} is (Xu et al., 2013; Lei et al., 2017):

$$S_{wc} = \frac{\int_{r_{min}}^{c0} f(r)\pi r^2 L_\tau dr}{\int_{r_{min}}^{c_{max}} f(r)\pi r^2 L_\tau dr} = \frac{r_{c0}^{3-D_T-D_f} - r_{min}^{3-D_T-D_f}}{r_{max}^{3-D_T-D_f} - r_{min}^{3-D_T-D_f}} \quad (1)$$

where r is pore radius; f is pore size distribution; L_τ is the length of tortuous capillary; D_f is the pore fractal dimension and D_T is the tortuosity fractal dimension. In addition, the subscript max represents the maximum; and min represents the minimum. Mathematically, based on fractal theory, we have (Yu and Li, 2001; Yu and Cheng, 2002; Lei et al., 2019a, 2019b)

$$\begin{cases} D_f = 2 + \dfrac{(D_{fn}-2)r_{maxn}}{(3-D_{fn})r_{max} + (D_{fn}-2)r_{maxn}} \\[2em] D_T = 1 + \dfrac{\ln\left\{\frac{1}{2}\left[1+\frac{1}{2}\sqrt{1-\varphi} + \dfrac{\sqrt{(1-\sqrt{1-\varphi})^2+\frac{1}{4}(1-\varphi)}}{1-\sqrt{1-\varphi}}\right]\right\}}{\ln\left(\dfrac{D_f-1}{\sqrt{D_f}}\sqrt{\dfrac{1-\varphi}{D_f}\dfrac{\pi}{2-D_f}}\dfrac{r_{max}}{r_{min}}\right)} \\[2em] f = D_f r_{min}^{D_f} r^{-(D_f+1)} \\[1em] L_\tau = (2r)^{1-D_T}L^{D_T} \\[1em] \quad = (2r)^{1-D_T}\left[\dfrac{\pi D_f r_{max}^2}{(2-D_f)r_{min}^{2-D_f}}(r_{max}^{2-D_f}-r_{min}^{2-D_f})\right]^{\frac{D_T}{2}} \end{cases}$$
$$(2)$$
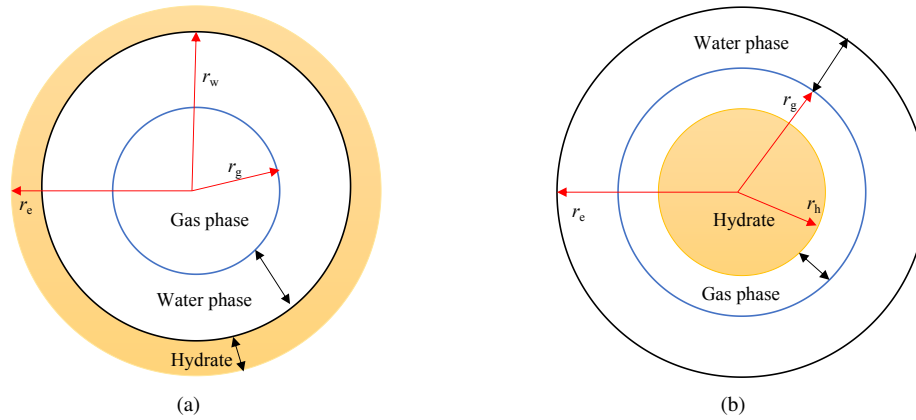
where D_{fn} is the pore fractal dimension of HBS under effective stress $p_{eff} = 0$; φ is the porosity; and the subscript *maxn* means the maximum value of HBS under effective stress $p_{eff} = 0$.

Eq. (1) reveals that residual water saturation S_{wc} changes with the change in hydrate saturation S_h. Specifically, for a given parameter r_{c0}, since parameters r_{max} and r_{min} decrease with the increasing of S_h, Eq. (1) suggests that residual water saturation will increase with the increasing of hydrate as parameter Sh increases. Physically, the critical pore radius r_{c0} in Eq. (1) is the function of varies parameters (clay minerals, clay content, and fluid physical properties). Based on Eq. (1), the critical pore radius r_{c0} is

$$r_{c0} = \left[(r_{max}^{3-D_T-D_f} - r_{min}^{3-D_T-D_f})S_{wc} + r_{min}^{3-D_T-D_f}\right]^{\frac{1}{3-D_T-D_f}} \quad (3a)$$

In this paper, we assume r_{c0} is independent on the effective stress, then, based on Eq. (3a), we have

$$r_{c0} = \left[(r_{maxn}^{3-D_{Tn}-D_f} - r_{minn}^{3-D_{Tn}-D_{fn}})S_{wc0} + r_{minn}^{3-D_{Tn}-D_{fn}}\right]^{\frac{1}{3-D_{Tn}-D_{fn}}} \quad (3b)$$

Fig. 3. Schematic of two main hydrate-growth patterns in hydrate-bearing sediments: (a) wall coating hydrates; (b) pore filling hydrates.

where S_{wc0} is the initial residual water saturation; D_{Tn} is the tortuosity fractal dimension of HBS under effective stress $p_{eff} = 0$; the subscript minn means the minimum value of HBS under effective stress $p_{eff} = 0$. More details about these parameters can be found in the former literature (Yu and Li, 2001; Yu and Cheng, 2002; Lei et al., 2017, 2019a, 2019b).

Singh et al. (2019) suggested that the amount of clays in HBS strongly affected the magnitude of bound-water saturation, thus affected the critical pore radius. Velocity equations for gas phase and water phase in a capillary with radius r_e will be :

$$\begin{cases} v_g = \dfrac{-\Delta p}{\mu_g L_\tau} \dfrac{r^2}{4} + c_1 \ln r + c_2 \\[3mm] v_w = \dfrac{-\Delta p}{\mu_w L_\tau} \dfrac{r^2}{4} + c_3 \ln r + c_4 \end{cases} \quad (4)$$

where v_g and v_w are gas phase velocity and water phase velocity, respectively; $c_1, c_2, c_3,$ and c_4 are integration constants; and μ_g and μ_w are gas phase viscosity and water phase viscosity, respectively.

Boundary conditions for WC hydrates are:

$$\frac{\partial v_g}{\partial r} = 0 \quad @r \to 0 \Rightarrow c_1 = 0 \quad (5a)$$

$$v_g = v_w @r = r_g \Rightarrow \frac{-\Delta p}{\mu_g L_\tau} \frac{r_g^2}{4} + c_1 \ln r_g + c_2$$
$$= \frac{-\Delta p}{\mu_w L_\tau} \frac{r_g^2}{4} + c_3 \ln r_g + c_4 \quad (5b)$$

$$\tau_g = \left(\mu_g \frac{\partial v_g}{\partial r} \right) = \tau_w = \left(\mu_w \frac{\partial v_w}{\partial r} \right) \quad (5c)$$

$$@r = r_g \Rightarrow \frac{-\Delta p r_g}{2 L_\tau} + \frac{\mu_g c_1}{r_g} = \frac{-\Delta r_g}{2 L_\tau} + \frac{\mu_w c_3}{r_g}$$

$$v_w = 0 \quad @r = r_w \Rightarrow \frac{-\Delta p}{\mu_g L_\tau} \frac{r_w^2}{4} + c_3 \ln r_w + c_4 = 0 \quad (5d)$$

and boundary conditions for PF hydrates are:

$$v_g = 0 \quad @r = r_h \Rightarrow \frac{-\Delta p}{\mu_g L_\tau} \frac{r_h^2}{4} + c_1 \ln r_h + c_2 = 0 \quad (5e)$$

$$v_g = v_w \quad @r = r_g \Rightarrow \frac{-\Delta p}{\mu_g L_\tau} \frac{r_g^2}{4} + c_1 \ln r_g + c_2$$
$$= \frac{-\Delta p}{\mu_w L_\tau} \frac{r_g^2}{4} + c_3 \ln r_g + c_4 \quad (5f)$$

$$\tau_g = \left(\mu_g \frac{\partial v_g}{\partial r} \right) = \tau_w = \left(\mu_w \frac{\partial v_w}{\partial r} \right) \quad (5g)$$

$$@r = r_g \Rightarrow \frac{-\Delta p r_g}{2 L_\tau} + \frac{\mu_g c_1}{r_g} = \frac{-\Delta r_g}{2 L_\tau} + \frac{\mu_w c_3}{r_g}$$

$$v_w = 0 \quad @r = r_e \Rightarrow \frac{-\Delta p}{\mu_g L_\tau} \frac{r_e^2}{4} + c_3 \ln r_e + c_4 = 0 \quad (5h)$$

where r is the radius, and the subscripts h, g, and w denotes hydrates, gas and water, respectively. μ_g and μ_w can be determined as (Gupta et al., 2017):

$$\begin{cases} \mu_g = 10.4 \times 10^{-6} \left(\dfrac{273.15 + 162}{T + 162} \right) \left(\dfrac{T}{273.15} \right)^{1.5} \\[3mm] \mu_w = 0.001792 \exp\left[-1.94 - 4.80 \left(\dfrac{T}{273.15} \right) \right. \\[2mm] \qquad \left. + 6.74 \left(\dfrac{T}{273.15} \right)^2 \right] \end{cases} \quad (6)$$

where T is temperature. Eq. (6) implies that μ_g is much lower than μ_w.

From Eqs. (4) and (5), the flow velocity equations for WC hydrates and PF hydrates are:

$$\begin{cases} v_g^{WC} = \dfrac{-\Delta p}{\mu_g L_\tau} \dfrac{r^2 - r_g^2}{4} + \dfrac{-\Delta p}{\mu_w L_\tau} \dfrac{r_g^2 - r_w^2}{4} & 0 < r \le r_g \\[3mm] v_w^{WC} = \dfrac{-\Delta p}{\mu_w L_\tau} \dfrac{r^2 - r_w^2}{4} & r_g < r \le r_w \end{cases} \quad (7)$$

and

$$\begin{cases} v_g^{PF} = \dfrac{-\Delta p}{\mu_g L_\tau}\dfrac{r^2-r_h^2}{4} + \dfrac{\Delta p}{4\mu_g L_\tau}\dfrac{r_g^2-r_h^2+\alpha(r_e^2-r_g^2)}{\ln(r_g/r_h)+\alpha\ln(r_e/r_g)}\ln\dfrac{r}{r_h} \\ \qquad\qquad\qquad r_h \le r \le r_g \\ v_w^{PF} = \dfrac{-\Delta p}{\mu_w L_\tau}\dfrac{r^2-r_e^2}{4} + \dfrac{\alpha\Delta p}{4\mu_g L_\tau}\dfrac{r_g^2-r_h^2+\alpha(r_e^2-r_g^2)}{\ln(r_g/r_h)+\alpha\ln(r_e/r_g)}\ln\dfrac{r}{r_e} \\ \qquad\qquad\qquad r_g \le r \le r_e \end{cases} \tag{8}$$

where $\alpha = \mu_g/\mu_w$ is the viscosity ratio. Integrating Eqs. (7) and (8), the gas-water volumetric flow rates in a single capillary for WC hydrates and PF hydrates are:

$$\begin{cases} q_g^{WC} = \displaystyle\int_0^{r_g} 2\pi r v_g dr = \dfrac{\Delta p \pi r_g^4}{8\mu_g L_\tau}\left[1-2\alpha\left(1-\dfrac{r_w^2}{r_g^2}\right)\right] \\ q_w^{WC} = \displaystyle\int_{r_g}^{r_w} 2\pi r v_w dr = \dfrac{\Delta p \pi}{8\mu_w L_\tau}\left(r_g^2-r_w^2\right)^2 \end{cases} \tag{9}$$

and

$$\begin{cases} q_g^{PF} = \displaystyle\int_{r_h}^{r_g} 2\pi r v_g^{PF} dr \\ \quad = \dfrac{\Delta p \pi}{8\mu_g L_\tau}\left\{-(r_g^2-r_h^2)^2 + \dfrac{r_g^2-r_h^2+\alpha(r_e^2-r_g^2)}{\ln(r_g/r_h)+\alpha\ln(r_e/r_g)}\right. \\ \qquad\qquad \left.\times\left[2r_g^2\ln\left(\dfrac{r_g}{r_h}\right)-(r_g^2-r_h^2)\right]\right\} \\ q_w^{PF} = \displaystyle\int_{r_g}^{r_e} 2\pi r v_w^{PF} dr \\ \quad = \dfrac{\Delta p \pi}{8\mu_w L_\tau}\left\{(r_e^2-r_g^2)^2 + \dfrac{r_g^2-r_h^2+\alpha(r_e^2-r_g^2)}{\ln(r_g/r_h)+\alpha\ln(r_e/r_g)}\right. \\ \qquad\qquad \left.\times\left[2r_g^2\ln\left(\dfrac{r_g}{r_h}\right)-(r_e^2-r_g^2)\right]\right\} \end{cases} \tag{10}$$

Based on Eqs. (2), (9) and (10), the total gas-water volumetric flow rates for WC hydrates and PF hydrates in HBS are (Yu et al., 2003; Lei et al., 2019b):

$$\begin{cases} Q_g^{WC} = \left(\dfrac{r_{\max}}{r_{\min}}\right)^{D_f}\displaystyle\int_{r_{c0}}^{r_{\max}} f(r_e)q_g^{WC}dr_e \\ \quad = \dfrac{\pi\Delta p D_f r_{\max}^{D_f}}{\mu_g 2^{4-D_T}L^{D_T}}\displaystyle\int_{r_{c0}}^{r_{\max}} r_g^4\left[1-2\alpha\left(1-\dfrac{r_w^2}{r_g^2}\right)\right]r_e^{D_T-D_f-2}dr_e \\ Q_w^{WC} = \left(\dfrac{r_{\max}}{r_{\min}}\right)^{D_f}\displaystyle\int_{r_{c0}}^{r_{\max}} f(r_e)q_w^{WC}dr_e \\ \quad = \dfrac{\pi\Delta p D_f r_{\max}^{D_f}}{\mu_w 2^{4-D_T}L^{D_T}}\displaystyle\int_{r_{c0}}^{r_{\max}} (r_g^2-r_w^2)^2 r_e^{D_T-D_f-2}dr_e \end{cases} \tag{11}$$

and

$$\begin{cases} Q_g^{PF} = N\displaystyle\int_{r_{c0}}^{r_{\max}} q_g^{PF} f(r_e)dr_e \\ \quad = \dfrac{\pi\Delta p D_f r_{\max}^{D_f}}{\mu_g 2^{4-D_T}L^{D_T}}\displaystyle\int_{r_{co}}^{r_{\max}} r_e^{D_T-D_f-2} \\ \qquad \left\{-(r_g^2-r_h^2)^2 + \dfrac{r_g^2-r_h^2+\alpha(r_e^2-r_g^2)}{\ln(r_g/r_h)+\alpha\ln(r_e/r_g)}\right. \\ \qquad \left.\left[2r_g^2\ln\left(\dfrac{r_g}{r_h}\right)-(r_g^2-r_h^2)\right]\right\}dr_e \\ Q_w^{PF} = N\displaystyle\int_{r_{c0}}^{r_{\max}} q_w^{PF} f(r_e)dr_e \\ \quad = \dfrac{\pi\Delta p D_f r_{\max}^{D_f}}{\mu_w 2^{4-D_T}L^{D_T}}\displaystyle\int_{r_{co}}^{r_{\max}} r_e^{D_T-D_f-2} \\ \qquad \left\{(r_g^2-r_g^2)^2 + \dfrac{r_g^2-r_h^2+\alpha(r_e^2-r_g^2)}{\ln(r_g/r_h)+\alpha\ln(r_e/r_g)}\right. \\ \qquad \left.\left(2r_g^2\ln\left(\dfrac{r_e}{r_g}\right)-(r_w^2-r_g^2)\right)\right\}dr_e \end{cases} \tag{12}$$

According to the distribution of three phases in a capillary with radius r larger than r_{c0} (Fig. 3), the saturations of hydrates, gas, and water in a capillary for WC hydrates and PF hydrates can be expressed as:

$$\begin{cases} S_{he}^{WC} = 1-\dfrac{r_w^2}{r_e^2}, \quad S_{ge}^{WC} = \dfrac{r_g^2}{r_e^2}, \quad S_{we}^{WC} = \dfrac{r_w^2-r_g^2}{r_e^2} \\ S_{he}^{PF} = \dfrac{r_h^2}{r_e^2}, \quad S_{ge}^{PF} = \dfrac{r_g^2-r_h^2}{r_e^2}, \quad S_{we}^{PF} = 1-\dfrac{r_g^2}{r_e^2} \end{cases} \tag{13}$$

Using Eq. (13), Eqs. (11) and (12) can be rearranged as:

$$\begin{cases} Q_g^{WC} = \dfrac{\pi\Delta p D_f r^{D_{f\max}}\left[(S_{ge}^{WC})^2+2\alpha S_{ge}^{WC}S_{we}^{WC}\right]}{\mu_g 2^{4-D_T}L^{D_T}} \\ \qquad\times\dfrac{r_{\max}^{D_T-D_f+3}-r_{c0}^{D_T-D_f+3}}{D_T-D_f+3} \\ Q_w^{WC} = \dfrac{\pi\Delta p D_f r^{D_{f\max}}(S_{we}^{WC})^2}{\mu_w 2^{4-D_T}L^{D_T}}\dfrac{r_{\max}^{D_T-D_f+3}-r_{c0}^{D_T-D_f+3}}{D_T-D_f+3} \end{cases} \tag{14}$$

and

$$\begin{cases} Q_g^{PF} = \dfrac{\pi\Delta p D_f r_{\max}^{D_f}}{\mu_g 2^{4-D_T}L^{D_T}} \\ \qquad\times\displaystyle\int_{r_{c0}}^{r_{\max}} r^{D_T-D_f+2}\left\{-(S_{ge}^{PF})^2+MM[MN_0-S_{ge}^{PF}]\right\}dr \\ Q_w^{PF} = \dfrac{\pi\Delta p D_f r_{\max}^{D_f}}{\mu_w 2^{4-D_T}L^{D_T}} \\ \qquad\times\displaystyle\int_{r_{c0}}^{r_{\max}} r^{D_T-D_f+2}\left\{(S_{we}^{PF})^2+MM[MN_1-S_{we}^{PF}]\right\}dr \end{cases} \tag{15}$$

where

$$\begin{cases} MM = \dfrac{S_{ge}^{PF} + \alpha S_{we}^{PF}}{\ln\left[\sqrt{(S_{he}^{PF}+S_{ge}^{PF})/S_{he}^{PF}}\right] + \alpha\ln\left[\sqrt{1/(S_{he}^{PF}+S_{ge}^{PF})}\right]} \\[4mm] MN_0 = 2(S_{he}^{PF}+S_{ge}^{PF})\ln\left(\sqrt{\dfrac{S_{he}^{PF}+S_{ge}^{PF}}{S_{he}^{PF}}}\right) \\[4mm] MN_1 = 2(S_{he}^{PF}+S_{ge}^{PF})\ln\left(\sqrt{\dfrac{1}{S_{he}^{PF}+S_{ge}^{PF}}}\right) \end{cases}$$

(16)

Based on Eqs. (14) to (16) and absolute permeability stated in the appendix A , the gas-water relative permeability for WC hydrates and PF hydrates in porous media is:

$$\begin{cases} K_{rg}^{WC} = (S_{ge}^{WC})^3 + 2\alpha(S_{ge}^{WC})^2 S_{we}^{WC} \\[3mm] K_{rw}^{WC} = (S_{we}^{WC})^3 \end{cases}$$

(17)

and

$$\begin{cases} K_{rg}^{PF} = S_{ge}^{PF}\left\{-(S_{ge}^{PF})^2 + MM[MN_0 - S_{ge}^{PF}]\right\} \\[3mm] K_{rw}^{PF} = S_{we}^{PF}\left\{(S_{we}^{PF})^2 + MM[MN_1 - S_{we}^{PF}]\right\} \end{cases}$$

(18)

The saturations of hydrates, gas, and water in porous media are:

$$\begin{cases} S_h = S_{he}^{WC}(1-S_{wc}) \quad S_g = S_{ge}^{WC}(1-S_{wc}) \\[3mm] S_w = S_{we}^{WC}(1-S_{wc})+S_{wc} \\[3mm] S_h = S_{he}^{PF}(1-S_{wc}) \quad S_g = S_{ge}^{PF}(1-S_{wc}) \\[3mm] S_w = S_{we}^{PF}(1-S_{wc})+S_{wc} \end{cases}$$

(19)

Inserting Eq. (19) into Eqs. (16), (17) and (18), we have:

$$\begin{cases} K_{rg}^{WC} = \left(\dfrac{S_g}{1-S_{wc}}\right)^3 + 2\alpha\left(\dfrac{S_g}{1-S_{wc}}\right)^2\dfrac{S_w-S_{wc}}{1-S_{wc}} \\[4mm] K_{rw}^{WC} = \left(\dfrac{S_w-S_{wc}}{1-S_{wc}}\right)^3 \end{cases}$$

(20)

and

$$\begin{cases} K_{rg}^{PF} = \dfrac{S_g}{1-S_{wc}}\left\{-\left(\dfrac{S_g}{1-S_{wc}}\right)^2 + MM\left(MN_0 - \dfrac{S_g}{1-S_{wc}}\right)\right\} \\[4mm] K_{rw}^{PF} = \dfrac{S_w-S_{wc}}{1-S_{wc}}\left\{\left(\dfrac{S_w-S_{wc}}{1-S_{wc}}\right)^2 + MM\left(MN_1 - \dfrac{S_w-S_{wc}}{1-S_{wc}}\right)\right\} \end{cases}$$

(21)

where

$$\begin{cases} MM = \dfrac{1}{1-S_{wc}}\dfrac{S_g+\alpha(S_w-S_{wc})}{\ln\left(\sqrt{1+\dfrac{S_g}{S_h}}\right) - \alpha\ln\left(\sqrt{\dfrac{1-S_w}{1-S_{wc}}}\right)} \\[5mm] MN_0 = 2\dfrac{1-S_w}{1-S_{wc}}\ln\left(\sqrt{1+\dfrac{S_g}{S_h}}\right) \\[5mm] MN_1 = -2\dfrac{1-S_w}{1-S_{wc}}\ln\left(\sqrt{\dfrac{1-S_w}{1-S_{wc}}}\right) \end{cases}$$

(22)

Eqs. (20) through (22) show that the K_{rw} (or K_{rg}) is a function of residual water saturation, water saturation (or gas saturation), hydrate saturation, and viscosity ratio related to temperature. Then, by using a relative permeability statistical average method (Sing et al., 2019a, 2019b), the effective relative permeability for describing different hydrate-growth patterns can be expressed as:

$$\begin{cases} K_{rg} = (K_{rg}^{PF})^\lambda (K_{rg}^{WC})^{1-\lambda} \\[3mm] K_{rw} = (K_{rw}^{PF})^\lambda (K_{rw}^{WC})^{1-\lambda} \end{cases}$$

(23)

where λ is the proportion of PF in all growth patterns of hydrates, which can be determined by experimental tests. Physically, parameter λ varies in the range of 0 (i.e., WC hydrate) to 1 (i.e., PF hydrate). Moreover, parameter λ increases with the increasing of hydrate saturation (i.e., WC hydrates will change into PF hydrates as hydrate saturation increases).

3. Validation

In this section, the derived models are validated by comparing the calculated results to different experimental data sets. Firstly, a former model by Lei et al. (2015) are selected to validate our derived relative permeability model with hydrate saturation $S_h = 0$. Additionally, experimental results of K_{rw} in HBS are also utilized to validate the relative permeability model in HBS.
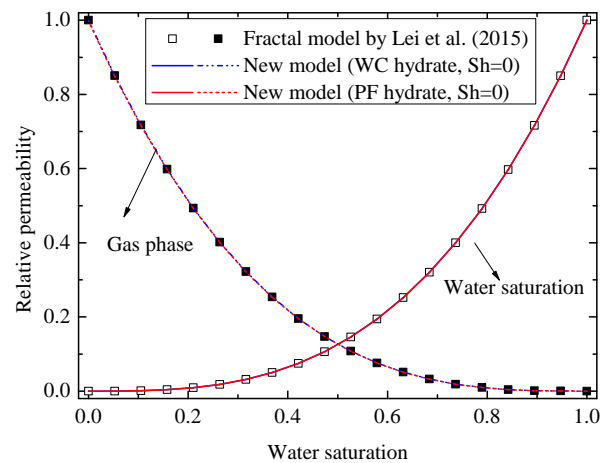

Fig. 4. Gas-water relative permeability in dry porous media without gas hydrates.

3.1 Gas-water relative permeability in dry porous media

Fig. 4 presents the comparison of the results from the fractal model by Lei et al. (2015) and the predictions from our derived model. When the immobile liquid film thickness δ in the fractal model is set to be 0, the fractal model can be used to calculate K_{rw} and K_{rg} in dry porous media without gas hydrates. In our derived model, the initial residual water saturation S_{wc0} is set to 0, the hydrate parameter S_h is set to 0, and p_{eff} is set to 0. The results (Fig. 4) indicate that the developed model is validated.
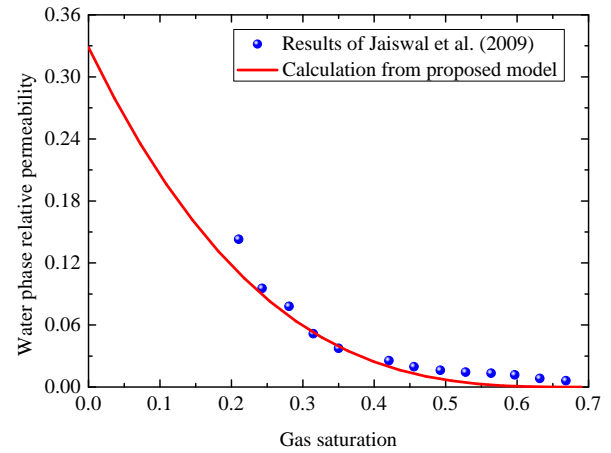
3.2 Water phase relative permeability in HBS

To further verify the derived model, we used experimental data from Jaiswal et al. (2009), who performed unsteady state gas-water relative permeability measurements on a synthetic sandstone sample with gas hydrate saturation of 0.31 in the Anadarko field. In the test, 2% brine was used to saturate the consolidated synthetic sandstone sample under a flow rate of 0.04 ml/min. Then, high pressure cold methane of temperature 4.5 °C and pressure 950 ∼ 1250 psig (6.55 ∼ 8.62) MPa was injected into the sample with the optimal rate of 1.5 ml/min to form gas hydrates. After the formation of hydrates, porosity and permeability of porous media were 7.85% and 7.04×10^{-5} μm^2, respectively. Then, gas-water displacement tests were performed with the unsteady state method. In our proposed model, the parameter porosity φ is set to 7.85%, the initial residual water saturation is set to 0, and the effective stress is set to 0. In addition, the initial maximum radius $r_{\mathrm{maxn}} = 0.47$ μm, the initial minimum radius $r_{\mathrm{minn}} = 4.7 \times 10^{-3}$ μm, and hydrate saturation $S_h = 31\%$ are assigned to our model, which could ensure that the parameter K is 7.04×10^{-5} μm^2. Fig. 5 compares the measured K_{rw} to the predicted data. As shown in Fig. 5, the predicted results provide a good match over the entire range of data.

4. Discussion

After validation by exhaustive experimental data, this derived model was used for sensitivity analysis of relevant physical parameters (e.g., hydrate saturation, effective stress, initial residual water saturation, etc.) K_{rw} and K_{rg} of HBS under stress dependence.

Fig. 6 shows the relative permeability versus gas saturation with different hydrate saturation. One can also see that gas-water relative permeability in PF hydrates is generally lower than that in WC One can also see that, under the same saturation, K_{rg} and K_{rw} in PF hydrates are generally lower than those in WC hydrates. Fig. 6(a) also reveals that, for WC hydrates (i.e., $\lambda = 0$), with a given gas saturation, a larger K_{rw} corresponds to a lower hydrate saturation, whereas the effect of hydrate S_h on K_{rg} is not significant. In contrast, Fig. 6(b) shows that, for PF hydrates (i.e., $\lambda = 1$), with a given gas saturation, both water phase relative permeability and gas phase relative K_{rw} and K_{rg} decline as hydrate saturation increases. In general, with the increasing of S_h, the pore sizes will become narrower,

Fig. 5. Relative permeability of water in porous media in the presence of hydrates. Effective stress is set to 0, parameter λ is set to 0 (i.e., WC hydrates), and parameter D_{fn} is set to 1.45.

and the wettability of water phase increases. Physically, with increasing wetting by the water, the intersection of the non-wetting and water relative permeabilities shifts to smaller nonwetting phase saturation (or the larger water saturation), and the maximum K_{rw} decreases. Similar results are shown in Fig. 6. In addition, Fig. 6(b) shows that K_{rw} firstly increases and then decreases as gas saturation increases. This can be interpreted as that, during gas-water flow in HBS, the water phase (i.e., fluid with relative higher viscosity) flows past the gas phase (i.e., fluid with relative lower viscosity). With lower gas saturation, the flow of the water phase, to some extent, can be regarded as a sliding motion in which low-viscosity fluid (gas phase) provides lubrication (Odeh, 1959; Ehrlich, 1993; Shad and Gates, 2010) (see Fig. 3(b)). For WC hydrates, however, K_{rw} monotonically decreases with the increasing of gas saturation, because the gas phase is no longer between the water phase and the hydrates (see Fig. 3(a)).

Since the parameter S_{wc0}, to some extent, represents the relative strength of wettability (Singh, 2019a), the derived model can be applied to investigate the effect of wettability on relative permeability. Fig. 7 shows relative permeability curves with different initial residual water saturations for hydrate saturations equal to 0.2 and 0.4. It is clear that a larger initial residual water saturation corresponds to a higher K_{rg} and a lower K_{rw}. Results presented in Fig. 7 also suggest that K_{rg} increases as wettability increases, while K_{rw} decreases as wettability increases. Similar observations were also reported in (Singh, 2019a). Moreover, it can also be seen from Fig. 7 that both K_{rg} and K_{rw} decline as S_h increases. Similar results are shown in Fig. 6.

Fig. 8 presents relative permeability curves with different effective stress (for $0 \leq p_{eff} \leq 15$ MPa). In our proposed model, residual water saturation is set to 0.1, rock elastic modulus is set to 8 GPa, and Poisson's ratio is set to 0.25. Fig. 8 shows that, under the given effective stress, K_{rg} increases with increasing effective stress, while K_{rw} decreases with the increase of p_{eff}. This finding is consistent with observations in other theoretical and experimental works (Lei et al., 2017).

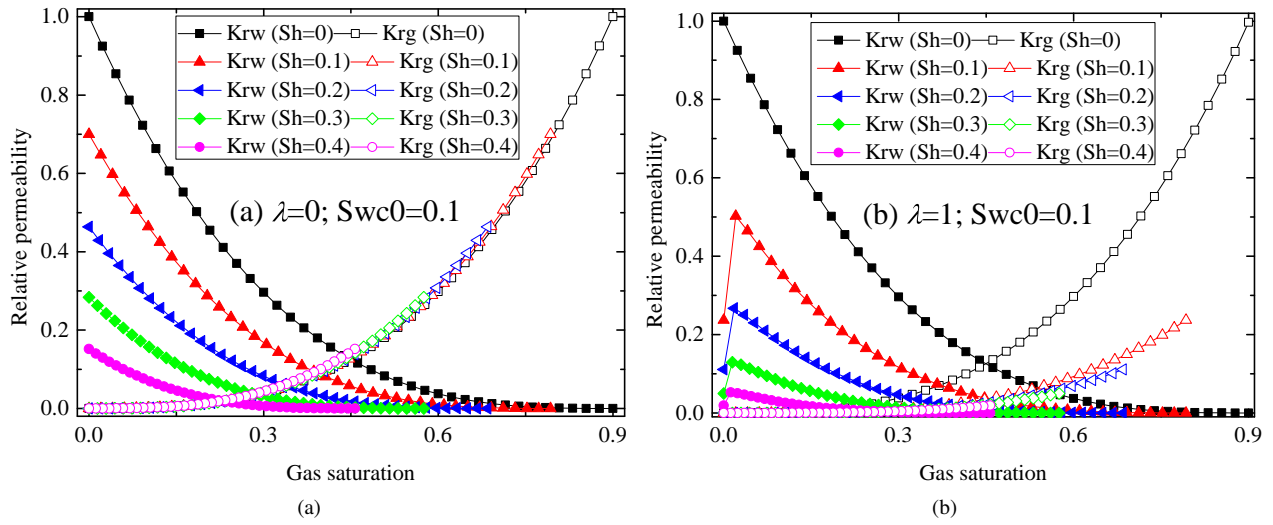Fig. 9 presents relative permeability curves with different

Fig. 6. Relative permeability versus gas saturation in HBS with different hydrate saturations. Effective stress is set to 0, and initial residual water saturation is set to 0.1.
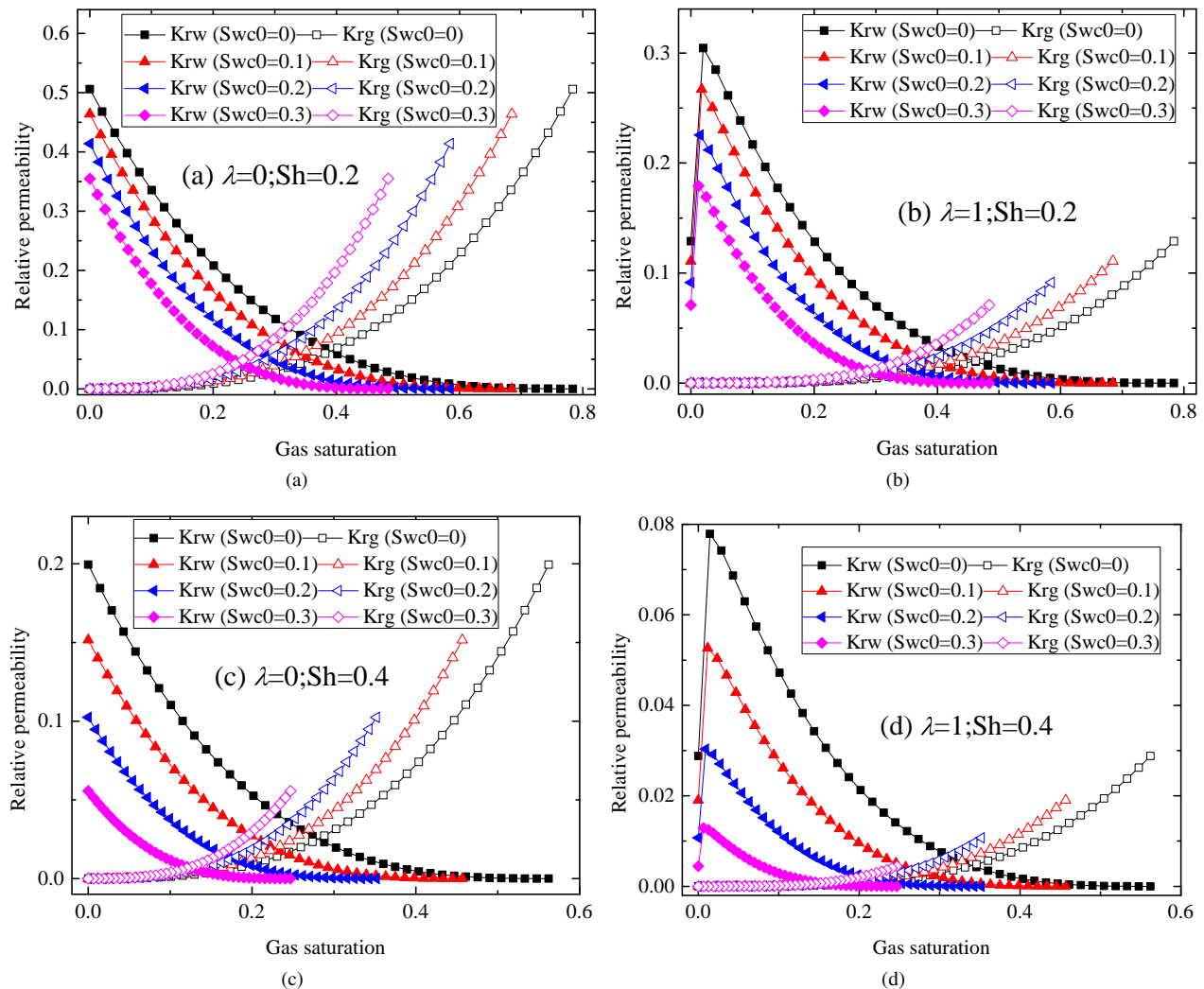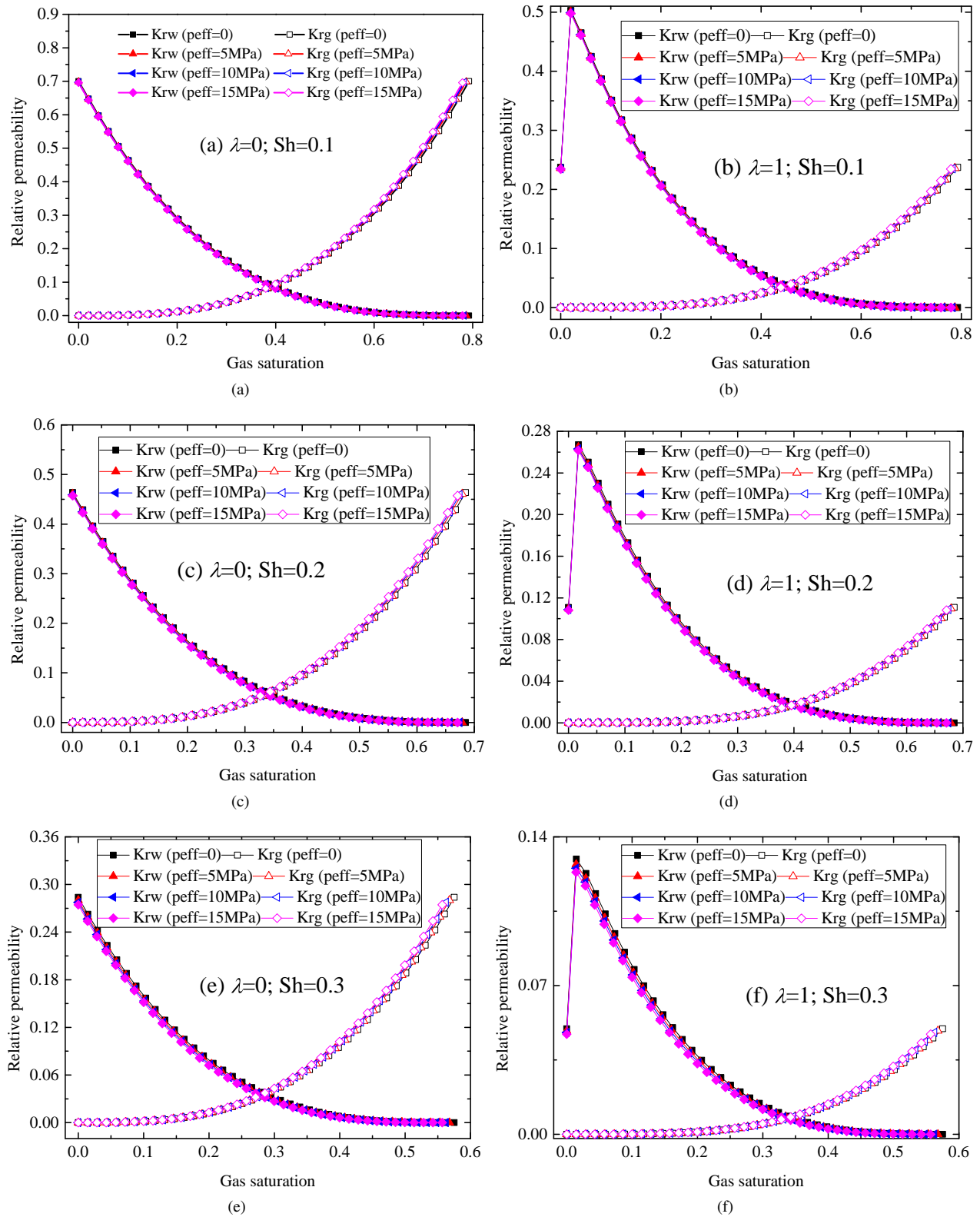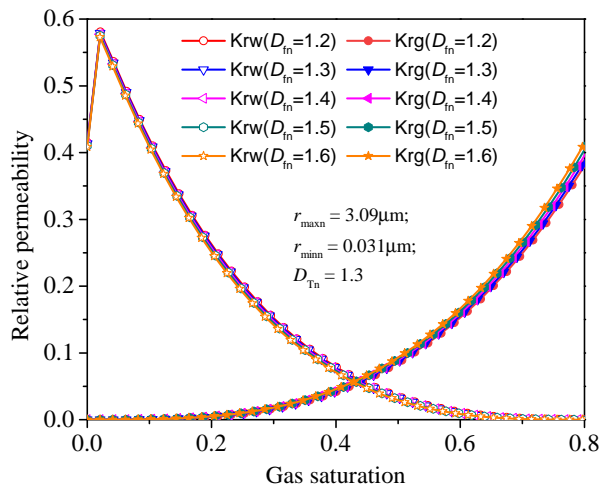

Fig. 7. Relative permeability versus gas saturation in porous media with different initial residual water saturation. Effective stress is set to 0.

Fig. 8. Relative permeability versus gas saturation in porous media with different effective stress. Initial residual water saturation is set to 0.1.

Fig. 9. Relative permeability in HBS with different D_{fn}. Hydrate saturation is set to 0.1, initial residual water saturation is set to 0.1, parameter λ is set to 0.5.

parameter D_{fn} (for $1.2 \leq D_{fn} \leq 1.6$). In the modeling, relevant parameters are assigned as follows: $r_{maxn} = 3.09$ μm; $r_{minn} = 0.031$ μm; $D_{Tn} = 1.3$; effective stress $p_{eff} = 10$ MPa; rock elastic modulus $E = 14.4$ GPa, and Poisson's ratio $\nu = 0.25$. As seen from Fig. 9, for a specific fluid saturation, K_{rw} decreases as the D_{fn} increases, while K_{rg} increases as the D_{fn} increases. The reason is that, a larger D_{fn} replies a more complex pore structure and a larger percent of small pores, leading to larger water phase flow resistance. Similar findings can be seen in other theoretical works (Xu et al., 2013; Lei et al., 2015).

5. Advantages and limitations of the derived model

The proposed relative permeability predictive model lays theoretical foundations for characterizing gas-water flow in deformable HBS. In addition, by combing inverse modeling, it can help to determine the pore-scale parameters with higher accuracy and the rock lithology. However, it is limited to capillary bundle model. Moreover, the derived model only accounts for PF hydrates and wall WC hydrates, and ignores other types (i.e., GC hydrates, lenses, and veins).

Results from this study suggest that, the effect of parameter λ (the proportion of pore filling in all growth patterns of hydrates) on the relative permeability prediction is significant. Physically, with the increasing of hydrate saturation, WC hydrates will change into PF hydrates. Thus, parameter λ increases as hydrate saturation increases. In general, experiment test is a good way to get the actual results. However, parameter λ in this work is predicted using the inverse modeling, and the quantitative relation between parameter λ and hydrate saturation is not determined. As a result, in this study, λ may cause uncertainty in the prediction, even though our predicted relative permeability is agreement with the test data. Consequently, further researches are required to reduce the uncertainty and make the model more accurate.

Moreover, in general, the residual water saturation changed dynamically with the change in hydrate saturation. However, in

this work, However, the quantitative relation between residual water saturation and hydrate saturation is not determined in previous literatures. Mathematically, our derived model Eq. (1) reveals that, for a given parameter r_{c0}, residual water saturation will increase with the increasing of hydrate saturation. Physically, parameter r_{c0} is related to hydrate saturation. However, the quantitative relation between parameter r_{c0} and hydrate saturation is not determined in this model. Consequently, further researches are needed to make the derived model more accurate.

6. Conclusion

In this paper, an analytical model is developed to investigate the stress-dependent water-gas relative permeability of hydrate-bearing sediments, which is validated by various experimental data and is shown to perform well. The existing relative permeability model without hydrate saturation is a special case of the derived model.

Gas-water relative permeability behavior in PF hydrates is significantly different from that in wall-coating WC hydrates. In addition, both gas phase and water phase relative permeabilities decline as hydrate saturation increases. As wettability increases, K_{rw} (relative permeability to wetting phase) decreases, while K_{rg} (relative permeability to non-wetting phase) increases. These findings suggest that, due to many factors in this complex system, we should be cautious in analyzing fluid flow in HBS.

In addition to providing theoretical foundations for quantifying relative permeability in HBS, another advantage of this derived stress-dependent permeability model is that, with experimental permeability data, it can be utilized to estimate pore-scale parameters and rock lithology using inverse modeling. Furthermore, the derived model can be applied as an alternative method for residual water saturation of deformable HBS determination, as nuclear magnetic resonance and special core analysis could be expensive and challenging. This work would provide a guidance to gas hydrates development.

Acknowledgement

Conflict of interest

The authors declare no competing interest.

References

Aya, I., Yamane, K., Nariai, H. Solubility of CO_2 and density of CO_2 hydrate at 30 MPa. Energy 1997, 22(2): 263-271.

Berge, L.I., Jacobsen, K.A., Solstad, A. Measured acoustic

wave velocities of R11 (CCl3F) hydrate samples with and without sand as a function of hydrate concentration. J. Geophys. Res. 1999, 104(7): 15415-15424.

Cui, Y., Lu, C., Wu, M., et al. Review of exploration and production technology of natural gas hydrate. Adv. Geo-Energy Res. 2018, 2(1): 53-62.

Dai, S., Santamarina, J.C., Waite, W.F., et al. Hydrate morphology: Physical properties of sands with patchy hydrate saturation. J. Geophys. Res. 2012, 117(B11): B11205.

Daigle, H. Relative permeability to water or gas in the presence of hydrates in porous media from critical path analysis. J. Pet. Sci. Eng. 2016, 146: 526-535.

Delli, M., Grozic, J. Experimental determination of permeability of porous media in the presence of gas hydrates. J. Pet. Sci. Eng. 2014, 120: 1-9.

Delli, M., Grozic, J. Prediction performance of permeability models in gas-hydrate-bearing sands. SPE J. 2013, 18(2): 274-284.

Dickens, G.R. Rethinking the global carbon cycle with a large, dynamic and microbially mediated gas hydrate capacitor. Earth Planet. Sci. Lett. 2003, 213(3): 169-183.

Ehrlich, R. Viscous coupling in two-phase flow in porous media and its effect on relative permeabilities. Transp. Porous Media 1993, 11(3): 201-218.

Fini, A., Garuti, M., Fazio, G., et al. Diclofenac salts. I. Fractal and thermal analysis of sodium and potassium diclofenac salts. J. Pharm. Sci. 2001, 90(12): 2049-2057.

Gallage, C., Kodikara, J., Uchimura, T. Laboratory measurement of hydraulic conductivity functions of two unsaturated sandy soils during drying and wetting processes. Soils Found. 2013, 53(3): 417-430.

Gupta, S., Deusner, C., Haeckel, M., et al. Testing a thermo-chemo-hydro-geomechanical model for gas hydrate-bearing sediments using triaxial compression laboratory experiments. Geochem. Geophys. Geosyst. 2017, 18(9): 3419-3437.

Helgerud, M.B. Wave speeds in gas hydrate and sediments containing gas hydrate: A laboratory and modeling study. Stanford, Stanford University, 2001.

Jaiswal, N.J., Dandekar, A.Y., Patil, S.L., et al. Relative permeability measurements of gas-water-hydrate systems, in Natural Gas Hydrates: Energy Resource Potential and Associated Geologic Hazard: AAPG Memoir 89, edited by T. Collett, A. Johnson and C. Knapp, et al., Tulsa, Oklahoma, pp. 723-733, 2009.

Ji, X., Chan, S., Feng, N. Fractal model for simulating the space-filling process of cement hydrates and fractal dimensions of pore structure of cement-based materials. Cem. Concr. Res. 1997, 27(11): 1691-1699.

Johnson, A., Patil, S., Dandekar, A. Experimental investigation of gas-water relative permeability for gas-hydrate-bearing sediments from the Mount Elbert Gas Hydrate Stratigraphic Test Well, Alaska North Slope. Mar. Pet. Geol. 2011, 28(2): 419-426.

Joseph, J., Singh, D.N., Kumar, P., et al. State-of-the-art of gas hydrates and relative permeability of hydrate bearing sediments. Mar. Georesour. Geotechnol. 2016, 34(5): 450-464.

Kang, D.H., Yun, T.S., Kim, K.Y., et al. Effect of hydrate nucleation mechanisms and capillarity on permeability reduction in granular media. Geophys. Res. Lett. 2016, 43(17): 9018-9025.

Kirchmeyer, W., Wyttenbach, N., Alsenz, J., et al. Influence of excipients on solvent-mediated hydrate formation of piroxicam studied by dynamic imaging and fractal analysis. Cryst. Growth Des. 2015, 15(10): 5002-5010.

Kleinberg, R.L., Flaum, C., Griffin, D.D., et al. Deep sea NMR: Methane hydrate growth habit in porous media and its relationship to hydraulic permeability, deposit accumulation, and submarine slope stability. J. Geophys. Res. 2003, 108(B10): 2508.

Kumar, A., Maini, B., Bishnoi, P.R., et al. Experimental determination of permeability in the presence of hydrates and its effect on the dissociation characteristics of gas hydrates in porous media. J. Pet. Sci. Eng. 2010, 70(1): 114-122.

Kvenvolden, K.A. A primer on the geological occurrence of gas hydrate. Geol. Soc. Lond Spec. Publ. 1998, 137(1): 9-30.

Kvenvolden, K.A. Methane hydrate-a major reservoir of carbon in the shallow geosphere? Chem. Geol. 1988, 71(1-3): 41-51.

Lee, H.J., Lee, J.D., Linga, P., et al. Gas hydrate formation process for pre-combustion capture of carbon dioxide. Energy 2010, 35(6): 2729-2733.

Lee, J., Lee, J., Kim, Y., et al. Stress-dependent and strength properties of gas hydrate-bearing marine sediments from the Ulleung Basin, East Sea, Korea. Mar. Pet. Geol. 2013, 47: 66-76.

Lei, G., Dong, P.C., Mo, S.Y., et al. A novel fractal model for two-phase relative permeability in porous media. Fractals 2015, 23(2): 1550017.

Lei, G., Dong, Z., Li, W., et al. A theoretical study on stress sensitivity of fractal porous media with irreducible water. Fractals 2017, 26(1): 1850004.

Lei, G., Li, W., Wen, Q. The convective heat transfer of fractal porous media under stress condition. Int. J. Therm. Sci. 2019, 137: 55-63.

Lei, G., Liao, Q., Patil, S., et al. Effect of clay content on permeability behavior of argillaceous porous media under stress dependence: A theoretical and experimental work. J. Pet. Sci. Eng. 2019, 179: 787-795.

Li, C., Zhao, Q., Xu, H., et al. Relation between relative permeability and hydrate saturation in Shenhu area, South China Sea. Appl. Geophys. 2014, 11(2): 207-214.

Liang, H., Song, Y., Chen, Y., et al. The measurement of permeability of porous media with methane hydrate. Pet. Sci. Technol. 2011, 29(1): 79-87.

Liu, L., Dai, S., Ning, F., et al. Fractal characteristics of unsaturated sands-implications to relative permeability in hydrate-bearing sediments. J. Nat. Gas Sci. Eng. 2019, 66: 11-17.

Liu, L., Zhang, X., Lu, X. Review on the permeability of hydrate-bearing sediments. Adv. Earth Sci. 2012, 27(7): 733-746.

Liu, L., Zhang, Z., Li, C., et al. Hydrate growth in quartzitic sands and implication of pore fractal characteristics to hydraulic, mechanical, and electrical properties of hydrate-bearing sediments. J. Nat. Gas Sci. Eng. 2020, 75: 103109.

Liu, W., Wu, Z., Li, Y., et al. Experimental study on the gas phase permeability of methane hydrate-bearing clayey sediments. J. Nat. Gas Sci. Eng. 2016, 36: 378-384.

Mahabadi, N., Dai, S., Seol, Y., et al. The water retention curve and relative permeability for gas production from hydrate-bearing sediments: pore-network model simulation. Geochem. Geophys. Geosyst. 2016, 17(8): 3099-3110.

Mahabadi, N., Zheng, X., Jang, J. The effect of hydrate saturation on water retention curves in hydrate-bearing sediments. Geophys. Res. Lett. 2016, 43(9): 4279-4287.

Masuda, Y. Numerical calculation of gas production performance from reservoirs containing natural gas hydrates. Paper SPE 38291 Presented at the SPE Annual Technical Conference, San Antonio, Texas, October, 1997.

Minagawa, H., Ohmura, R., Kamata, Y., et al. Water permeability of porous media containing methane hydrate as controlled by the methane-hydrate growth process, in Natural Gas Hydrates: Energy Resource Potential and Associated Geologic Hazard: AAPG Memoir 89, edited by T. Collett, A. Johnson and C. Knapp, et al., Tulsa, Oklahoma, pp. 734-739, 2009.

Nimblett, J., Ruppel, C. Permeability evolution during the formation of gas hydrates in marine sediments. J. Geophys. Res. 2003, 108(B9): 2420.

Odeh, A.S. Effect of viscosity ratio on relative permeability (includes associated paper 1496-G). Trans. AIME 1959, 216(1): 346-353.

Ordonez, C., Grozic, J.L.H., Chen, J. Hydraulic conductivity of Ottawa sand specimens containing R-11 gas hydrates. Paper Presented at the 62nd Canadian Geotechnical Conference, Halifax, 2009.

Waite, W.F., Santamarina, J.C., Cortes, D.D., et al. Physical properties of hydrate-bearing sediments. Rev. Geophys. 2009, 47: RG4003.

Wang, J., Zhao, J., Zhang, Y., et al. Analysis of the influence of wettability on permeability in hydrate-bearing porous media using pore network models combined with computed tomography. J. Nat. Gas Sci. Eng. 2015, 26: 1372-1379.

Shad, S., Gates, I.D. Multiphase flow in fractures: co-current and counter-current flow in a fracture. J. Can. Pet. Technol. 2008, 49(2): 48-55.

Singh, H. Representative elementary volume (REV) in spatio-temporal domain: a method to find REV for dynamic pores. J. Earth Sci. 2017, 28(2): 391-403.

Singh, H., Mahabadi, N., Myshakin, E.M., et al. A mechanistic model for relative permeability of gas and water flow in hydrate-bearing porous media with capillarity. Water Resour. Res. 2019, 55(4): 3414-3432.

Singh, H., Myshakin, E.M., Seol, Y. A nonempirical relative permeability model for hydrate-bearing sediments. SPE J. 2019, 24(2): 547-562.

Sloan, E.D. Gas hydrates: Review of physical/chemical properties. Energy Fuels 1998, 12(2): 191-196.

Stoll, R.D., Bryan, G.M. Physical properties of sediments containing gas hydrates. J. Geophys. Res. 1979, 84(B4): 1629-1634.

Sun, Y., Lu, H., Lu, C., et al. Hydrate dissociation induced by gas diffusion from pore water to drilling fluid in a cold wellbore. Adv. Geo-Energy Res. 2018, 2(4): 410-417.

Tajima, H., Yamasaki, A., Kiyono, F. Energy consumption estimation for greenhouse gas separation processes by clathrate hydrate formation. Energy 2004, 29(11): 1713-1729.

Terzariol, M., Goldsztein, G., Santamarina, J.C. Maximum recoverable gas from hydrate bearing sediments by depressurization. Energy 2017, 141: 1622-1628.

Xu, P., Qiu, S., Yu, B., et al. Prediction of relative permeability in unsaturated porous media with a fractal approach. Int. J. Heat Mass Transf. 2013, 64: 829-837.

Yang, L., Ai, L., Xue, K., et al. Analyzing the effects of inhomogeneity on the permeability of porous media containing methane hydrates through pore network models combined with CT observation. Energy 2018, 163: 27-37.

Yousif, M.H., Abass, H.H., Selim, M.S., et al. Experimental and theoretical investigation of methane-gas-hydrate dissociation in porous media. SPE Reserv. Eng. 1991, 6(1): 69-76.

Yu, B., Cheng, P. A fractal permeability model for bi-dispersed porous media. Int. J. Heat Mass Transf. 2002, 45(14): 2983-2993.

Yu, B., Li, J. Some fractal characters of porous media. Fractals 2001, 9(3): 365-372.

Yu, B., Li, J., Li, Z., et al. Permeabilities of unsaturated fractal porous media. Int. J. Multiph. Flow 2003, 29(10): 1625-1642.

Zhang, W., Ye, J., Wang, Y., et al. Pore structure and surface fractal characteristics of calcium silicate hydrates contained organic macromolecule. J. Chin. Ceram. Soc. 2006, 34(12): 1497-1502.

Zhang, Z., Li, C., Ning, F., et al. Pore fractal characteristics of hydrate-bearing sands and implications to the saturated water permeability. J. Geophys. Res. 2020, 125(3): e2019JB018721.

Zhao, Y., Guo, K., Liang, D., et al. Formation process and fractal growth model of HCFC-141b refrigerant gas hydrate. Sci. China-Chem. 2002, 45(2): 216-224.

Zheng, R., Li, S., Li, Q., et al. Study on the relations between controlling mechanisms and dissociation front of gas hydrate reservoirs. Appl. Energy 2018, 215: 405-415.

Appendix A: Fractal permeability model of HBS under stress conditions

Based on fractal theory, absolute permeability K of porous media is (Xu et al., 2013; Lei et al., 2017)

$$\begin{cases} K = \dfrac{D_f r_{\max}^{D_f - D_T - 1} \pi}{2^{4-D_T} \left[\dfrac{\pi D_f}{2-D_f} \left(\dfrac{r_{\max}^{2-D_f}}{r_{\min}^{2-D_f}} - 1 \right) \right]^{\frac{D_T+1}{2}}} \dfrac{r_{\max}^{3+D_T-D_f} - r_{c0}^{3+D_T-D_f}}{3+D_T-D_f} \end{cases} \tag{A-1}$$

where the maximum (or minimum) stress dependent pore radius $r_{\max}$ (or $r_{\min}$) can be written as (Lei et al., 2019a, 2019b)

$$\begin{cases} r_{\max}(P_{eff}) = r_{\max n} \left\{ 1 - 4 \left[\dfrac{3\pi(1-v^2)p_{eff}}{4E} \right]^{\beta} \right\} \\ r_{\min}(P_{eff}) = r_{\min n} \left\{ 1 - 4 \left[\dfrac{3\pi(1-v^2)p_{eff}}{4E} \right]^{\beta} \right\} \end{cases} \tag{A-2}$$

where E denotes the Young's modulus, v is the Poisson's ratio, and β denotes the parameter representing the rough pore surface.